Taylor & Francis
Taylor & Francis Group

Automatika

Journal for Control, Measurement, Electronics, Computing and Communications

ISSN: (Print) (Online) Journal homepage: https://www.tandfonline.com/loi/taut20

Design of a Partial Resonant Inverter for solar photovoltaic applications

C Vidhya, S Muralidharan & V Ravikumar

To cite this article: C Vidhya, S Muralidharan & V Ravikumar (2021) Design of a Partial Resonant Inverter for solar photovoltaic applications, Automatika, 62:3-4, 434-448, DOI: 10.1080/00051144.2021.1983697

To link to this article: https://doi.org/10.1080/00051144.2021.1983697

© 2021 The Author(s). Published by Informa UK Limited, trading as Taylor & Francis Group

Published online: 27 Sep 2021.

Submit your article to this journal

Article views: 338

View related articles

View Crossmark data

Full Terms & Conditions of access and use can be found at
https://www.tandfonline.com/action/journalInformation?journalCode=taut20

AUTOMATIKA
2021, VOL. 62, NOS. 3–4, 434–448
https://doi.org/10.1080/00051144.2021.1983697

REGULAR PAPER

OPEN ACCESS Check for updates

Design of a Partial Resonant Inverter for solar photovoltaic applications

C Vidhya[a], S Muralidharan[a] and V Ravikumar[b]

[a]Electrical and Electronics Engineering Department, Kalasalingam Institute of Technology, Krishnankoil, India; [b]Electrical and Electronics Engineering Department, Mepco Schlenk Engineering College, Sivakasi, India

ABSTRACT

This paper presents a solar-powered Partial Resonant Inverter (PRI) interfaced with an asymmetrical cascaded nine-level inverter. The DC input of the proposed system is obtained using Solar Photovoltaic (SPV) panel. The input DC sources fed to the asymmetrical cascaded nine-level inverter are in the ratio of 1:3. The step modulated nine-level inverter works with a precalculated switching angle for a fixed modulation of 0.7. Compared to the conventional 50 Hz inverter and the multi-output transformer design, the proposed system is more compact because of the high-frequency AC link. The PRI ensures Zero Voltage Switching (ZVS) and reduces the switching losses. The proposed scheme has been validated in the MATLAB/ SIMULINK environment and an experimental prototype is built in the laboratory. Based on the investigations the Selective Harmonic Elimination (SHE) method gives superior performance when compared to the Optimal Harmonic Stepped Modulation (OHSM) method. From the results and comparative analysis, the proposed system uses fewer switches to obtain the nine-level output, uses the PRI setup with the multioutput transformer to make the design compact and improves the power quality of the system.

ARTICLE HISTORY
Received 29 October 2020
Accepted 16 September 2021

KEYWORDS
Partial Resonant Inverter; solar photovoltaic; asymmetric; nine-level inverter; Selective Harmonic Elimination

1. Introduction

Cascaded H bridge Multilevel Inverters (CHBMLI) are used in various applications since they use isolated DC power supplies, individually for each of the H bridges [1]. If all the H-bridges of CHBMLI use unequal DC voltages, then such a configuration is known as the Asymmetrical Multilevel Inverter (AMLI) [2]. In the case of a five-level inverter, the two H bridges of CHBMLI are powered by two isolated DC sources which are in the ratio of 1:2. To obtain a nine-level output the DC sources must be in the ratio of 1:3 [3]. Conventionally isolated DC sources are obtained by [4] using a multi-winding transformer with a diode bridge rectifier (DBR). Implementation of the setup makes the system bulky and heavy since the isolation transformer with multiple output windings operates at 50 Hz.

A comprehensive review of Multilevel Inverters and their reduced structures has been presented in [5]. The authors in [6] introduced a novel structure with PV panels for grid applications. In [7] the authors have proposed and validated a reduced switch MLI with multiple solar PV panels. The drawback of the presented work is based on the maximum power point tracking (MPPT). MPPT has to be applied to all the panels and it becomes a hectic overload. The MLIs using cascaded H bridges often encounter the problem of unequal voltage drops due to the usage of isolated DC sources. This drawback seriously affects the power quality at the output of the inverter [8]. The main assumption considered in the design of an MLI usually includes symmetric DC sources. However, in practice, it is not so, and it needs special attention to maintain the DC voltages for the cascaded H bridges at the desired levels [9]. The authors in [10] implemented a cascaded control for the grid integrated modular inverter. The superior performance makes the modular inverter feed harmonic less current to the grid. In [11] the authors have proposed three configurations of PV-based resonant inverters. They are high-frequency inverter (HFI) with cycloconverter, HFI-rectifier-PWM (pulse width modulation) voltage source inverter (VSI), and HFI-rectifier- line commutated inverter. These topologies require multiple conversion stages. Moreover, large inductors are needed for the DC current link and large capacitors are needed for the DC link. In [12] the authors introduced a resonant inverter that uses 12 bidirectional switches. The ac link inverter uses the pulse density modulation method (PDM)for switching the 12 bidirectional switches. An HFI based on the buck–boost concept is implemented in [13]. It uses four unidirectional and six bidirectional switches. This topology offers single-stage conversion and inherent isolation. The authors in [14] proposed a series partial resonant converter (SEPARC). The resonant circuit elements (Land C) are connected in series.

CONTACT C Vidhya vidhyamanju7337@gmail.com Electrical and Electronics Engineering Department, Kalasalingam Institute of Technology, Anand Nagar, Krishnankoil, India

© 2021 The Author(s). Published by Informa UK Limited, trading as Taylor & Francis Group
This is an Open Access article distributed under the terms of the Creative Commons Attribution License (http://creativecommons.org/licenses/by/4.0/), which permits unrestricted use, distribution, and reproduction in any medium, provided the original work is properly cited.

Table 1. Comparison with various resonant inverter topologies from literature.

Ref	Topology	Tank circuit	N_{sw}	§	ϕ	€	η
[12]	HF-AC-link-Inverter	L and C in parallel	24	ZVS	Small	Yes	Low
[13]	AC-link buck-boost converter	L and C in parallel	16	ZVS	Small	Yes	High
[14]	SEPARC	L and C in series	20	ZCS	Large	No	Low
[15]	Multiport HF-AC-link-Inverter	L and C in parallel	24	ZVS	Small	Yes	Low
[16]	Universal Power Converter	L and C in parallel	20	ZVS	Medium	Yes	Low
[17]	Sparse ac-link buck boost inverter	L and C in parallel	18	ZVS	Small	Yes	High
[18]	Ultra-Sparse ac-link buck boost inverter	L and C in parallel	10	ZVS	Very small	Yes	High
[19]	Extreme-Sparse	L and C in parallel	14	ZVS	Very small	Yes	High

N_{sw}: number of switches; §: switching strategy; ϕ: circulating Energy; €: Light Load Voltage Regulation; η: efficiency.

This topology enables zero current switching and does not require bulky capacitors and transformers. In [15] the authors presented a multiport HFI. The proposed system has 16 stages of operation, of which 8 stages are resonating stages and the remaining 8 are power transfer stages. Galvanic isolation can be achieved by replacing the inductor (L) with an HF transformer. In [16] the author patented a universal power converter know as a partial resonant converter (PARC). The PARC consists of 20 switches and is capable of converting DC power to AC power using a parallel LC resonant circuit. The use of HF AC-link reduces the size of the capacitor and transformer in the circuit. In [17] the authors proposed a modified PARC with the reduction in the number of switches. The proposed inverter is also known as a sparse ac-link buck–boost inverter. It consists of 18 switches and can be built using IGBTs. It is cheaper, less complicated to control and compact. In [18] and [19] the authors have proposed an Ultra Sparse and Extreme Sparse ac-link buck–boost inverter which uses only 10 and 14 switches. The ultra-sparse circuit has four additional diodes which increase the losses in the system. Table 1 presents the comparison of the various resonant inverter topologies discussed in the literature.

From Table 1 it is observed that most of the topologies use zero voltage switching (ZVS) and the switch count of various topologies have been reduced. Greater switch count leads to losses in the system thereby reducing the efficiency of the system. In [13,17,18,19] even though the switches are reduced, the output power from the inverter contains harmonics. Therefore, in the proposed system a partial resonant converter with reduced switch AMLI is implemented for improving the power quality at the output of the inverter. To improve the power quality at the output of the inverter a suitable PWM method has to be implemented. There have been many contributions in the area of switching angle estimation for the step modulated multilevel inverters. Optimization techniques have been widely used in the estimation of step angles for multilevel inverters [20]. The authors in [21] have demonstrated the implementation of a neural network with training data derived from a genetic algorithm-based (GA) optimization. The authors in [22] have adopted the Particle Swarm Optimization (PSO) for estimation of the switching angles for a five-level inverter. A Modified Hopfield Neural Network (MHNN) has also been used for the estimation of the switching angles in a three-level inverter [23].

For standalone applications as well as the grid integrated multilevel inverters, the quality of power injected should be of sufficient level [24]. Henceforth, the DC voltages across the DC rails of the H bridge inverters are maintained constant and the inverter is run with a fixed modulation index to get a harmonic less AC output.

The sliding mode control (SMC) is used in the solar PV panel to retrieve the maximum output from the PV panel. The partial resonant inverter (PRI) associated with the solar PV panel converts the DC power available from the PV panel into AC power. In order to control the proposed system and to maintain the voltage levels at the desired ratio, a closed-loop control strategy is implemented with the help of SMC. The PRI works only if the SMC gives the command to the PRI.

2. Topological description

In the proposed work, a regulated and isolated set of two DC voltage sources suitable for driving the nine-level AMLI is designed. The block diagram shown in Figure 1 uses a single Solar PV panel with a DC-to-DC boost converter followed by a PRI and a parallel resonant AC link at the front end. A set of two HF transformers are used after the partial resonant AC link and these transformers drive two Diode Bridge Rectifiers (DBR), which deliver the required DC voltages across the DC link capacitors of two cascaded H bridge inverter units. The DC link voltages are in the ratio of 1:3 and these DC link voltages are controlled by establishing the closed-loop control. An SMC is provided for regulating the DC link voltages at the desired level.

A generic boost converter is used at the front end where the MPPT control for the Solar PV panel is implemented using the SMC technique. The front-end boost converter delivers power to an intermediate DC link where a battery is connected in parallel. The role of a battery is to provide the required backup power during the absence and inadequacy of solar power. The PRI is driven from this DC link.

The PRI ensures ZVS and reduces the switching losses occurring at the semiconductors of the PRI. Since the resonant AC link has a high frequency (1.35 KHz),

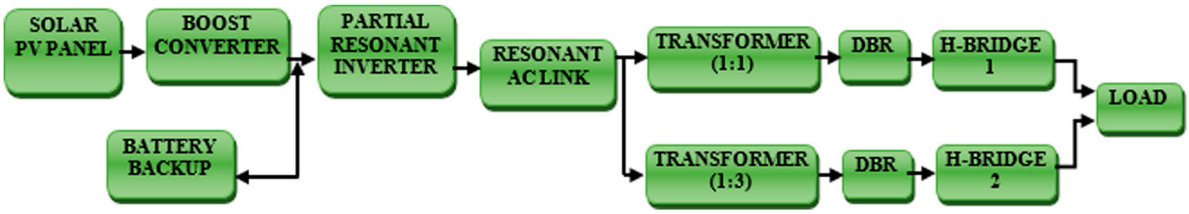

Figure 1. Block diagram of the proposed system.

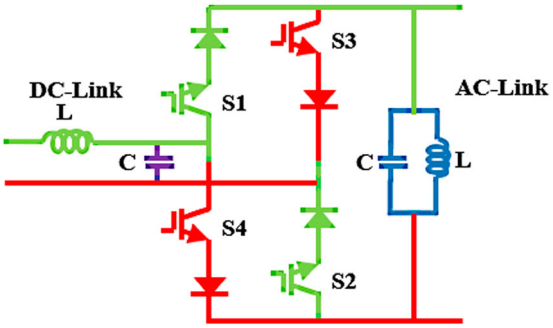

Figure 2. Topology of PRI.

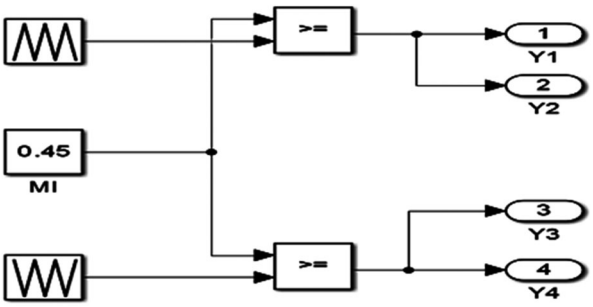

Figure 3. PRI switching generation unit.

the size of the transformer gets reduced. The transformer's structure is inversely proportional to the operating frequency and the flux density [25]. Therefore, reduced size and weight can be gained by the high-frequency operation of the magnetic core.

As the size of the transformer gets reduced, the core of the transformer becomes small, lightweight and the whole system becomes compact. The proposed idea has been validated in the MATLAB/SIMULINK platform and an experimental prototype with a 125W solar photovoltaic power source has also been developed.

3. Partial Resonant Inverter

The PRI is a single-phase inverter with a parallel resonant circuit across the output terminals of the inverter. The topology of the PRI is shown in Figure 2. The topology of the PRI is similar to that of the conventional H bridge inverter. In addition, there are four diodes, each of which is connected in series with the semiconductor switches. Further, unlike the conventional inverter, in the PRI, the DC source is connected across the nodes of the inverter and the resonant AC output is available across the rails.

The four power electronic switches of the PRI are switched by the switching pulses obtained from the control circuit. The IGBTs S1, S2, S3, and S4 are switched ON or OFF simultaneously.

The switches in the same leg (S1, S4, and S3, S2) are not switched ON simultaneously. The circuit arrangement for producing the switching pulses is shown in Figure 3. There is a facility for controlling the amplitude of the output of the PRI by controlling the modulating index (MI). The frequency of oscillation of the AC link voltage appearing across the parallel LC circuit is given by,

$$f_o = \frac{1}{2\pi\sqrt{\mathrm{LC}}} \tag{1}$$

where $L = 14\mathrm{mH}$ and $C = 1\mu\mathrm{f}$. Substituting the values of L and C in Equation (1), $f_o = 1.35\mathrm{KHz}$. Hence, a frequency of 1.35 KHz is used for resonating the AC link circuit

4. SMC based MPPT

A solar PV panel is used in the proposed system to supply DC power to the entire system. Due to the nonlinear characteristics [26] of the solar PV system, maximum power cannot be extracted from the PV panels. For extracting maximum power from the PV systems various maximum power point tracking (MPPT) methods are used. The maximum power point tracking scheme ensures that the maximum possible power is derived from the solar panel, by the real-time changes in the climatic conditions, like solar irradiance and temperature, which influence the power generation of the PV panel.

The authors in [27] surveyed various conventional and recently developed MPPT methods. The authors in [28] integrated the artificial intelligence approach in MPPT, which eventually increased the efficiency of the PV system. In the proposed system the input power is drawn from a solar PV panel, therefore a suitable MPPT technique is essential to harvest maximum power from the PV panel. MPPT has been implemented in the front-end generic boost converter. The SMC [29] based MPPT is preferred in the proposed system as it requires only one real-time parameter, that is the voltage across the PV panel, to be measured. Figure 4 shows the characteristics of the solar PV panel for constant irradiance of 950 $\mathrm{W/m^2}$ and change in irradiance of 950 to

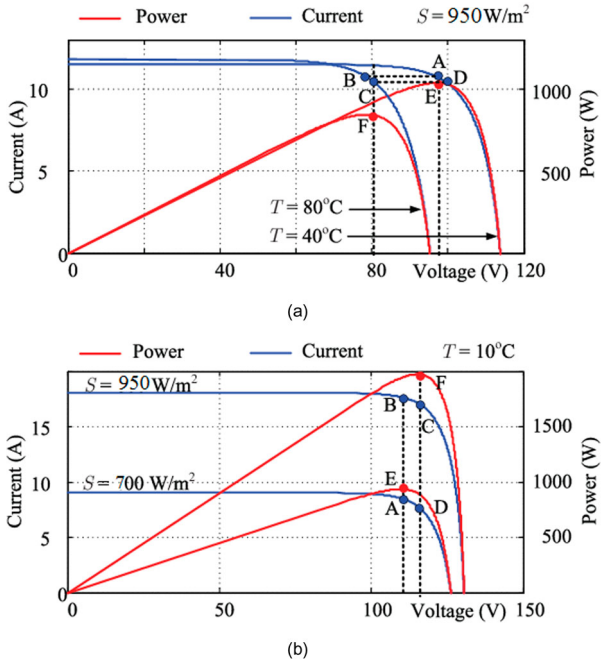

Figure 4. Simulated I-V and P-V characteristics of PV array, (a) at constant solar irradiance 950W/m2 (b) at constant temperature 10°C.

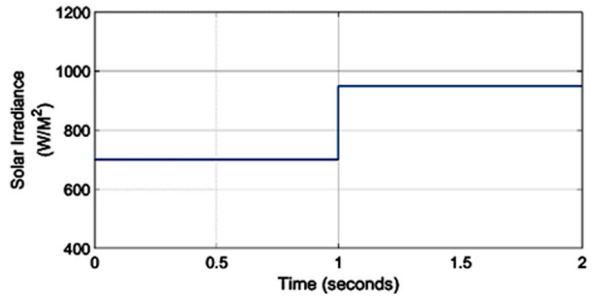

Figure 5. Solar irradiance with a step change at 1 sec.

700 w/m^2. For the given environmental conditions, the harvested power is maximum only at a specific operating point, and at this point the terminal voltage of the PV panel and the PV panel current form a unique pair.

The solar PV panel drives the boost converter. The output of the boost converter makes the battery charge. Suddenly if the solar insolation is increased from 700 to 950 W/m^2, then the battery current starts increasing irrespective of the battery voltage. Figure 5 presents the step change in the insolation level from 700 to 950 W/m^2. Figure 6 presents the change in the battery current from 5A to 7A due to a change in the insolation level. Figure 7 presents the terminal voltage across the battery.

For a PV panel, the ratio between the parameters V_{pmax} and V_{oc} is a constant k and this constant is valid for all climatic conditions namely any solar irradiance or any ambient temperature [30]. Therefore, for any given solar irradiance and temperature the ratio between V_{pmax} and V_{oc} is also a constant. If

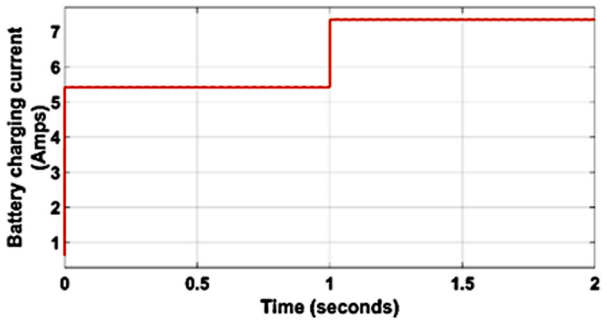

Figure 6. Change in the battery charging current with the change in the solar irradiance.

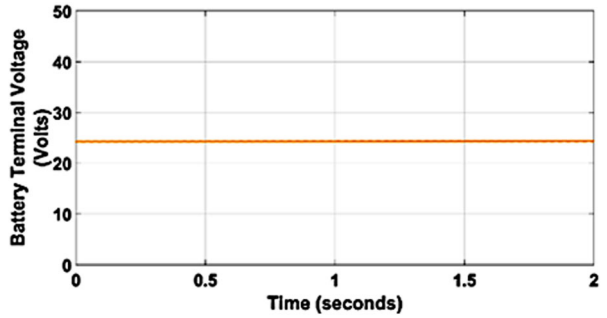

Figure 7. Terminal voltage across the battery.

the PV panel is loaded such that the prevailing terminal voltage V_{pv} across the panel maintains this ratio with the open-circuit voltage for the given conditions then maximum power is harvested for the existing climatic condition. Based on this principle the SMC-based MPPT is operated. The SMC is a nonlinear controller which is suitable for nonlinear systems. In the case of SMC, the manipulated parameter is pushed between two extremes such that the deviation of the controlled parameter from the desired value is pushed towards the set value such that the controlled parameter is always within the acceptable vicinity of the set value [31]. For example, by the application of the SMC the controlled parameter may swing between positive and negative errors of 0.01 about the desired value. This tolerance can be adjusted to suit the requirement. In the case of the boost converter, the duty cycle is pushed between two extreme limits typically 0.1 and 0.5 so that the controlled parameter is just moving about the desired value with allowable tolerance.

The step-by-step implementation of the Sliding Mode Controlled MPPT scheme is given below:

Step 1. Keep the power electronic switch in the boost converter with a minimum duty cycle say 0.1. This keeps the solar panel in nearly no-load condition. (State = 0)

Step 2. Measure the voltage across the PV panel and it is V_{oc}.

Step 3. Increase the duty cycle to a high value, say 0.5. (State = 1) The voltage gain is now 2 and the solar PV panel is now loaded.
Step 4. Measure the terminal voltage across the PV panel.
Step 5. If $V_{pv} > k\ (V_{oc})$ keep State = 1 else go to step 1.

This basic algorithm is being used for obtaining the maximum power from the solar PV panel.

5. Modes of operation

The output power from the PV panel mainly depends on the irradiation and the temperature. A variation in the output power is observed when there is a change in the climatic condition. Therefore, the power delivered to the load also changes with changes in climatic conditions. To maintain the constant voltage across the DC link, battery backup is used.

The basic requirement of the battery is that it supports the system during nighttime and also during cloudy days. The battery is charged (during the peak solar insolation period) when the harvested solar PV power is more than the demand. The battery can also be charged during the light load or no-load conditions provided solar irradiation is available. On other hand, the battery gets discharged when there is no solar power.

The battery is rated at 35Ah and its nominal terminal voltage is 24V. The boost converter makes the battery charge from the solar PV source. The duty cycle and the voltage gain of the boost converter are considered as 0.5 and 2 respectively. Since the nominal PV panel voltage is 17.5V, the output of the boost converter will be 34V.

However, since the battery acts as a voltage sink and is also held up at a nominal voltage of 24V, the boost converter in its boost action drives the charging current against the voltage sink. Therefore, constant voltage with variable current is obtained and is directly used for charging the battery. Thus, possible scenarios of operation could be summarized as in Table 2.

6. Design equations of isolated DC sources

In the case of the cascaded multilevel inverters with equal voltage DC sources, the number of levels that could be obtained for the output voltage is given by Equation (2),

$$n = 2N + 1 \tag{2}$$

where N is the number of bridges and n is the number of voltage levels. To get an output voltage with nine-level the number of H bridges required is,

$$N = \frac{(n-1)}{2} \tag{3}$$

However, in the case of an asymmetrical nine-level inverter, even with less number of bridges more voltage levels can be obtained as shown in Equations (4) and (5).

If the DC sources are given by $V_k = 2^{(k-1)}$, number of levels in the output is,

$$n = 2^{(N+1)} \tag{4}$$

If the DC sources are given by $V_k = 3^{(k-1)}$, number of levels in the output is,

$$n = 3^N \tag{5}$$

where n is the number of levels in the output, N is the number of bridges and k is the index.

For example, with $V_k = 2^{(k-1)}$, the different voltages are in the ratio $1 : 2 : 4$ or $V_1 = 2^0 = 1$; $V_2 = 2^1 = 2$; and with $V_k = 3^{(k-1)}$ the different voltages are in the ratio $1 : 3 : 9$ or $V_1 = 3^0 = 1$; $V_2 = 3^1 = 3$ and $V_3 = 3^2 = 9$.

Thus, with two isolated DC sources, and two H bridges, if the voltages of the DC sources are in the ratio 1 : 2, the number of levels obtained in the inverter would be 7. Similarly, if the two DC source voltages are in the ratio 1 : 3, nine-level could be obtained at the inverter output. In this work, the proposed nine-level inverter has been developed with two H bridge inverter modules supplied by two isolated DC source voltages of ratio 1 : 3.

Table 2. Operating modes.

Component	Modes of operation				
Solar PV	GH		GM	NG	
Battery	Charging		MD	FRD	
Load	Full		Full	Full	
Battery Status	Full	Medium	Weak	Weak'	Medium
Solar PV	GH	GM	NG	GH	GM
Load	Full	Full	off	no load	no load
Battery mode	off	md	off	charge	charge

GH: generation high; GM: generation medium; NG: no generation; MD: medium discharge; FRD: full rated discharge.

7. Selective Harmonic Elimination

In selective harmonic elimination due to quarter-wave symmetry of a voltage wave, it is only necessary to find half of the angles $\boldsymbol{\alpha}_1, \boldsymbol{\alpha}_2, \boldsymbol{\alpha}_3, \ldots \boldsymbol{\alpha}_n$. To find the firing angles, the expansion of the Fourier series is analyzed, where Equation (6) is obtained.

$$H_n = \frac{4Vdc}{n\pi} \sum_{i=1}^{k} [\cos(\alpha_i)] \tag{6}$$

where H_n is the function of the output wave in terms of Fourier, V_{dc} is the voltage of the DC power supply, k is the number of switching angles, n is the odd harmonics and $\boldsymbol{\alpha_i}$ is the switching angle to be calculated. The switching angles should satisfy the limitations:

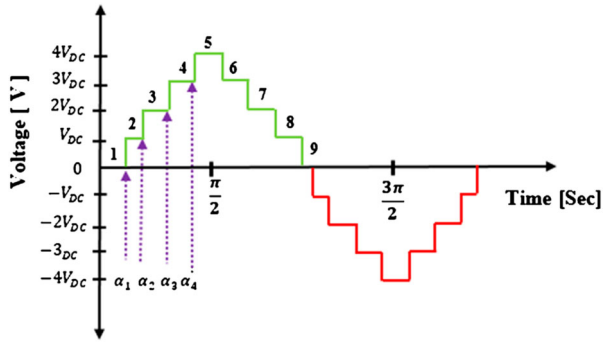

Figure 8. Implementation of SHE for the nine-level inverter.

$\alpha_1 < \alpha_2 < \alpha_3 < \alpha_4 < \frac{\pi}{2}$. For any inverter of "k" voltage levels, it is necessary to calculate "m = (k – 1)/2" switching angles, so for the nine-level inverter, it is necessary to calculate 4 switching angles. Solving Equation (6) gives the following system of nonlinear equations presented in Equation (7).

$$\begin{aligned}
&\mathrm{Cos}(\alpha_1) + \mathrm{Cos}(\alpha_2) + \mathrm{Cos}(\alpha_3) + \cos(\alpha_4) = \mathrm{M} \times \mathrm{F}\\
&\cos(3\alpha_1) + \cos(3\alpha_2) + \cos(3\alpha_3) + \cos(3\alpha_4) = 0\\
&\cos(5\alpha_1) + \cos(5\alpha_2) + \cos(5\alpha_3) + \cos(5\alpha_4) = 0\\
&\cos(7\alpha_1) + \cos(7\alpha_2) + \cos(7\alpha_3) + \cos(7\alpha_4) = 0 \quad (7)
\end{aligned}$$

where M is the modulation index and F is the number of inverter power supplies. By triggering the switches, a nine-level output is generated in which the third, fifth, and seventh order harmonics are minimized. By solving four nonlinear equations, four triggering angles are obtained. These triggering angles are stored in the lookup table and are fed as pulses to the switches of AMLI. Figure 8 presents the implementation of SHE for the nine-level inverter.

7.1. Calculation of switching angles

In order to solve the nonlinear equations in (7), and obtain the switching angles Hopfield Neural Network is used. The HNN method uses the energy function (Œ) to obtain the ordinary differential equations (ODEs) and the ODEs are further computed using the Runge–Kutta 4th order method[32].

$$\begin{aligned}
\text{Œ} = -2(&\cos(\alpha_1) - \cos(\alpha_2) + \cos(\alpha_3) - \cos(\alpha_4) - M)^2 + (\cos(3\alpha_1) - \cos(3\alpha_2) + \cos(3\alpha_3)\\
&- \cos(3\alpha_4))^2 + (\cos(5\alpha_1) - \cos(5\alpha_2) + \cos(5\alpha_3) - \cos(5\alpha_4))^2 + (\cos(7\alpha_1)\\
&- \cos(7\alpha_2) + \cos(7\alpha_3) - \cos(7\alpha_4))^2 \qquad (8)
\end{aligned}$$

From the nonlinear equations the switching angle is obtained using an energy function and is specified as follows

$$\begin{aligned}
\frac{d\alpha_1}{dt} &= -\frac{\partial E}{\partial \alpha_1}\\
\frac{d\alpha_2}{dt} &= -\frac{\partial E}{\partial \alpha_2}\\
\frac{d\alpha_3}{dt} &= -\frac{\partial E}{\partial \alpha_3}\\
\frac{d\alpha_4}{dt} &= -\frac{\partial E}{\partial \alpha_4} \qquad (9)
\end{aligned}$$

Equation (9) is solved using the Runge–Kutta 4th order method to obtain the switching angles. The step-by-step calculation of switching angles using the HNN method is shown in Appendix.

8. Simulation and experimental results

Figure 9 presents the simulation diagram of the proposed system. The high-frequency transformers with the two isolated secondary windings, along with the two sets of DBRs are also presented in Figure 9. The parameters used for simulation are shown in Table 3. The Simulink model of the PRI is shown in Figure 10. Figure 3 presents the switching pulses for the PRI. In Figure 3, it is shown that the switching pulses are generated with a fixed modulation index of 0.45. The DC link voltage of the H Bridge handling the higher voltage is 60 V. This 60 V is regulated by the SMC as shown in Figure 11.

Figures 12 and 13 show the switching pulses for the switching modules Y1, Y2 and Y3, and Y4. Figure 14 shows the waveform of the AC link voltage. The AC link resonates at 1.35KHz with an AC link voltage of 80 V. Figure 15 gives the information regarding the Partial Resonant nature of the AC link voltage. The two isolated DC voltages are obtained from the resonant AC

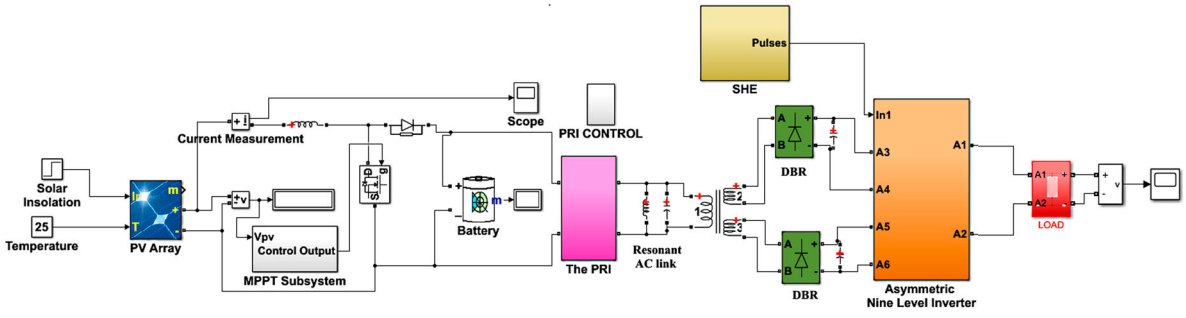

Figure 9. Simulation diagram of the proposed system.

Table 3. Simulation specifications.

Solar PV panel	
Nominal power output	125W
Open circuit voltage (V_{oc})	22.2V
Short circuit current (I_{oc})	8.2A
Maximum voltage (V_{pmax})	17.5V
Maximum current (I_{pmax})	7.4A
Partial Resonance Inverter	
IGBT	4 switches
Diode	4 diodes
Transformation Ratio of the Transformers	
Transformer 1	N1:N2 = 1:1
Transformer 2	N1:N2 = 1:3
Cascaded H bridge Inverter	
Nominal source voltage	V1 = 20 V (H bridge 1)
Nominal source voltage	V2 = 60 V (H bridge 2)
Miscellaneous Components	
Filter capacitor	C1 = 2200 µF, C2 = 2200µF
Load resistance	10 Ω
Load inductance	10 mH
Battery (Lead acid)	24 V,35Ah

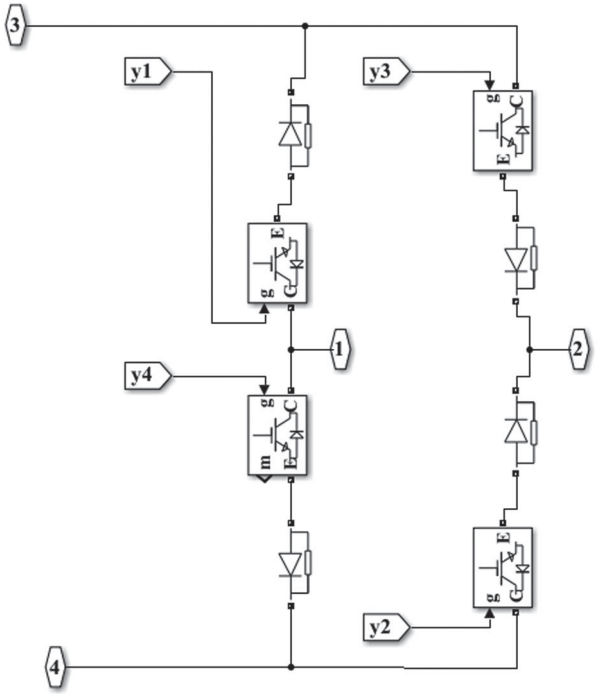

Figure 10. Simulink model of PRI.

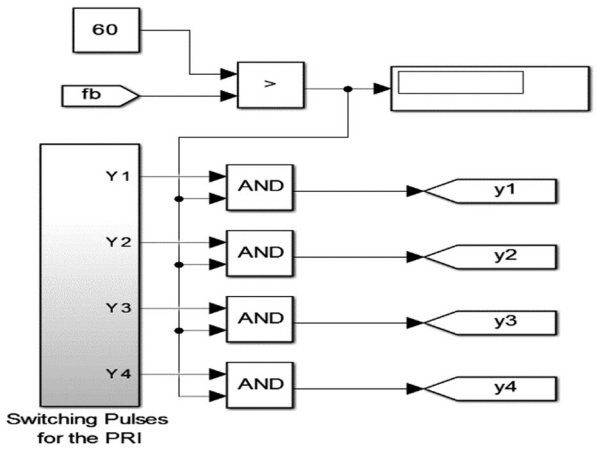

Figure 11. Switching Pulses for PRI.

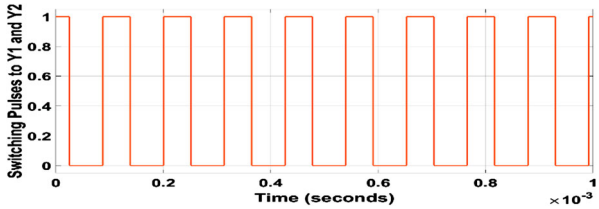

Figure 12. Switching Pulses for Y1 and Y2.

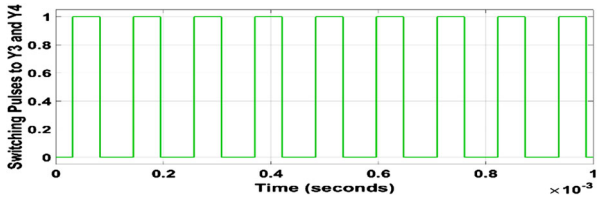

Figure 13. Switching Pulses for Y3 and Y4.

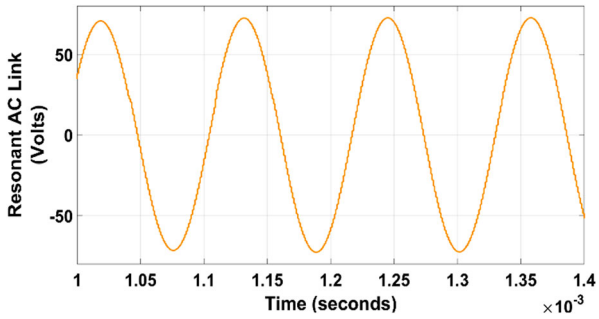

Figure 14. Resonant AC Link Voltage.

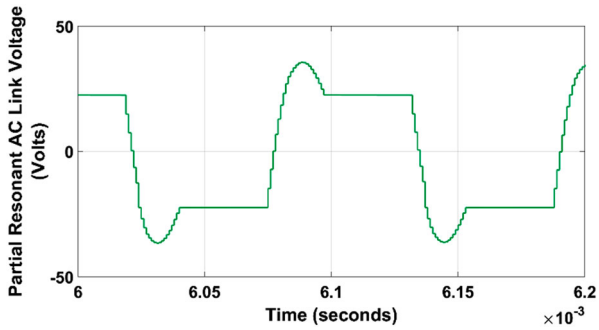

Figure 15. Partial Resonant AC Voltage across the output terminals of the PRI.

bus bar. Two ferrite core transformers are used and the primary of these transformers are connected across the resonant AC bus bar. These Two ferrite core transformers are wound with turns ratio 1:1 and 1:3. The output of the individual ferrite core transformer is separately rectified and two isolated DC voltages are obtained in the ratio of 1:3. Since the AC link resonates at a frequency of nearly 1.35 KHz, the filter capacitors used after the rectifiers are also small.

Two different modulation strategies have been implemented and the results have been obtained. The first strategy is the optimal harmonic stepped modulation (OHSM) scheme [33]. In OHSM the output voltage

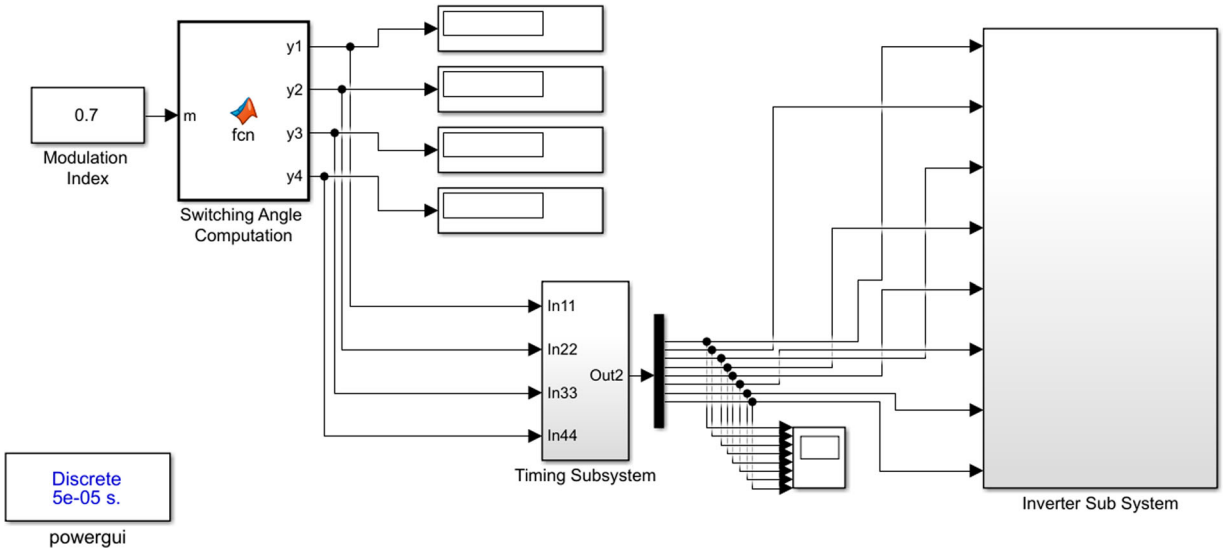

Figure 16. Execution of SHE in MATLAB.

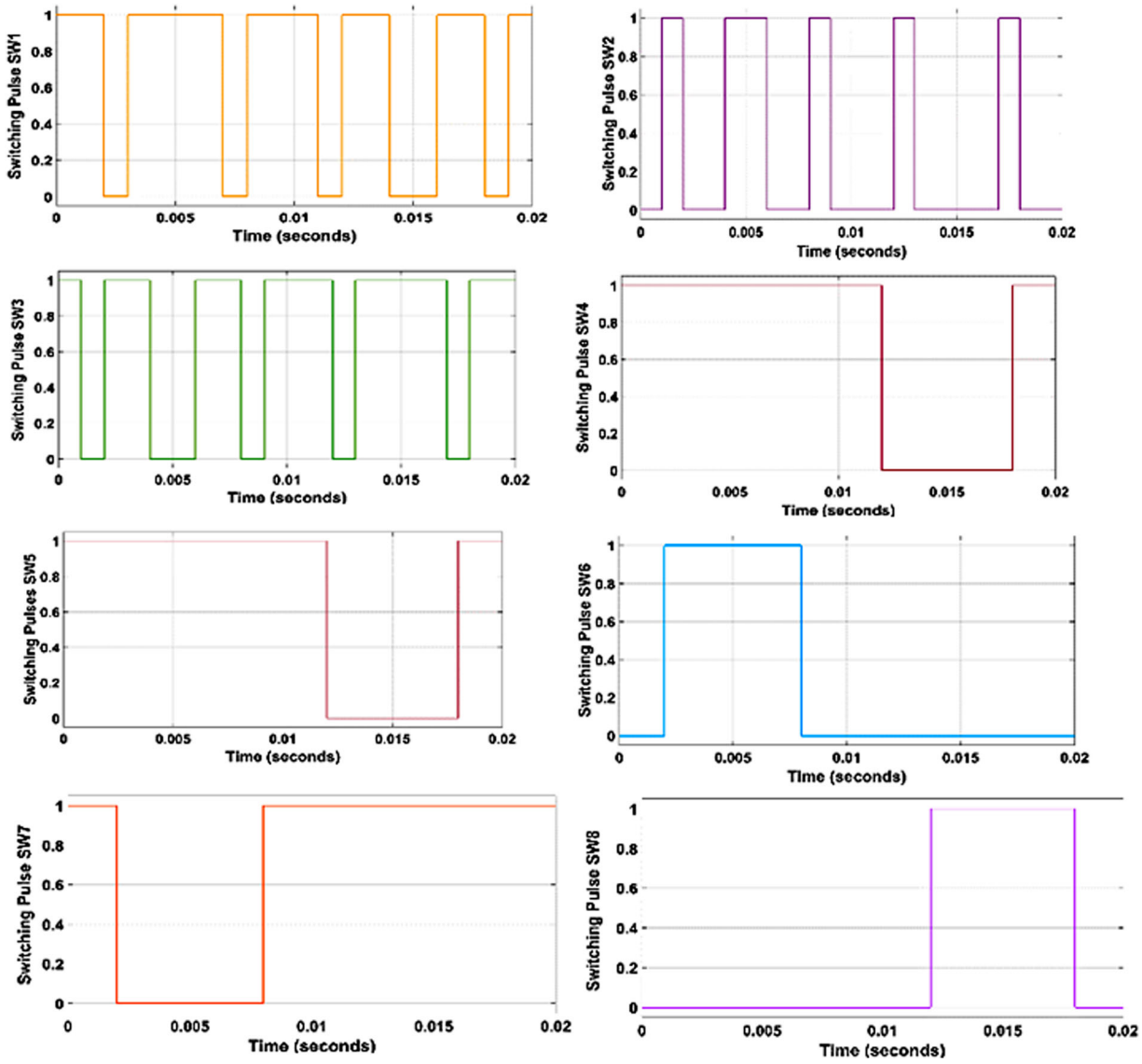

Figure 17. Switching pulses for the nine-Level Inverter.

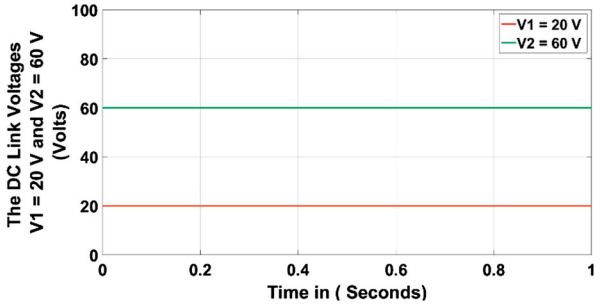

Figure 18. DC Link voltages in the 1: 3 ratio.

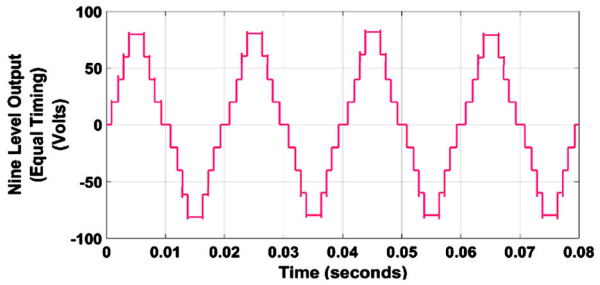

Figure 19. Nine Level Output Voltage with OHS PWM.

levels have been uniformly distributed over the entire period in each cycle.

Thus, a total of five level which includes 0, 1, 2, 3, 4 level in each quarter-wave period has been allotted uniformly for a period of 1 ms. Thus, a total period of 20 ms for each cycle has been allotted for all the levels uniformly divided in each of the four quarter cycles.

In the second strategy, the Selective Harmonic Elimination PWM scheme is adopted. The switching angles estimated using Hopfield Neural Network [32] have been developed for the nine-level inverter with a fixed modulation index of 0.7. Figure 16 shows the implementation of SHE in MATLAB for the proposed system. Figure 17 shows the pulses generated by the SHE method for the proposed asymmetric inverter.

Figure 18 shows the DC input to the asymmetric multilevel inverter. From Figure 18 it is observed that the DC input to the asymmetric multilevel inverter is maintained in the ratio of 1:3. The boost converter steps up the solar output voltage from 17.5 to 24 V. By the SMC-based closed-loop control system implemented in the PRI, the DC link voltages were maintained at 20 and 60 V respectively.

Figure 19 shows the output of the nine-level inverter using the optimal stepped harmonic modulation method. The harmonic spectrum of the output voltage is shown in Figure 20. From Figure 20 it is observed that the total harmonic distortion (THD) obtained is 10.46%, which is much higher than the IEEE519 standards. Figure 21 depicts the output voltage of the nine-level inverter with the SHE PWM method. The harmonic spectrum of the output voltage is shown in Figure 22. From Figure 22 it is observed that

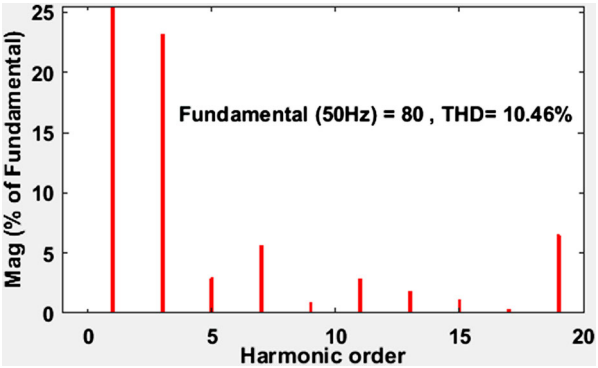

Figure 20. THD of the Output Voltage with OHS PWM.

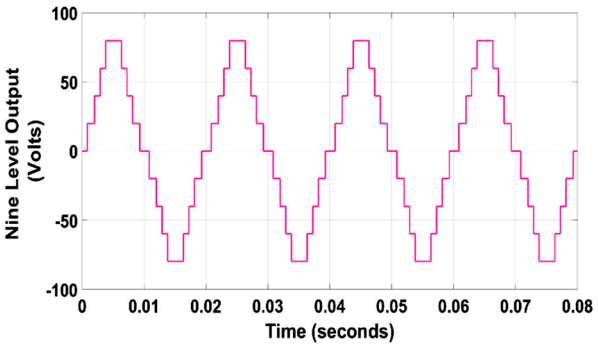

Figure 21. Nine Level Output Voltage with SHE PWM.

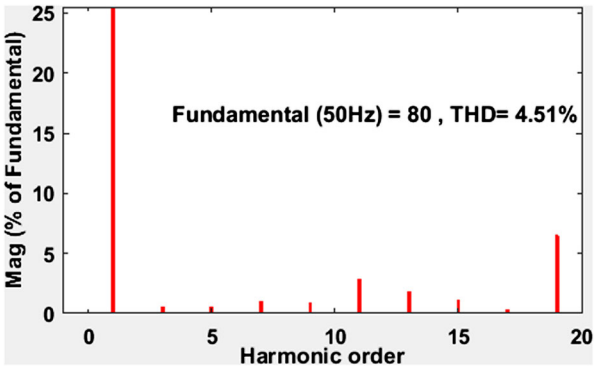

Figure 22. THD of the Output Voltage with SHE PWM.

the lower order harmonics of third, fifth, and seventh orders have been reduced in the output voltage and the THD content obtained is 4.51% which is very less and it satisfies the IEEE519 standards.

9. Experimental verification

Prototype of the proposed system is tested in the laboratory. Figure 23 shows the entire prototype of the proposed system. Figure 24 shows the prototype of the inverter module with capacitors and a programmed pulse generator. Figure 25 presents the prototype of the proposed system with PV panels. A generic boost converter is used for obtaining the isolated DC sources for the proposed system.

The boost converter uses the IRF 540 MOSFET, to harvest power from the solar PV panel and injects that

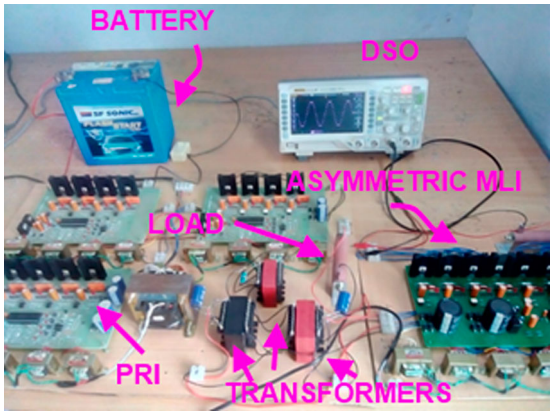

Figure 23. Overall Experimental Setup.

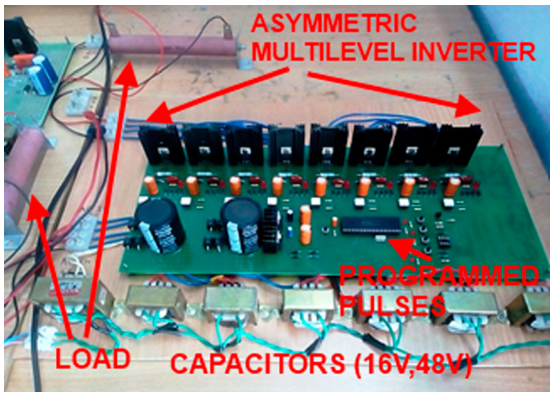

Figure 24. Prototype of the Nine Level Inverter Module.

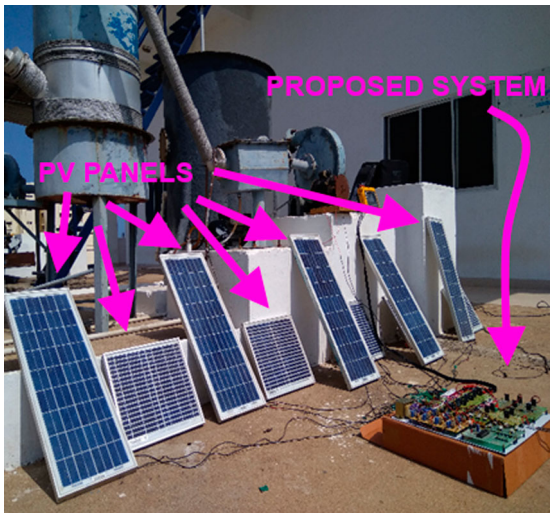

Figure 25. Experimental setup with PV input.

power to the intermediate DC Link. A 12 V battery is connected for backup and during the night hours or cloudy days when the solar PV is not available, the battery supplies power to the resonant AC link. The PRI contains four IRF 540 MOSFET, which is switched simultaneously to obtain power from the intermediate DC link and drives the resonant AC link. From the resonant AC link, the power is transferred to two H bridges

Table 4. Hardware specifications.

Controller	
Controller IC for the Nine Level Inverter	PIC 16F877A
Controller IC for the PRI	
Controller IC for the boost DC to DC Converter	
Opto Couplers	MCT 2E
Solar PV panel	
V_{oc}	22.2V
I_{sc}	8.2A
Vp_{max}	17.5V
I_{pmax}	7.14A
Boost converter	
Switch IRF No Switching frequency	5 KHz
Inductor	500 mH
Capacitor	2200 µF
Lead Acid Battery	12 V 35Ah
Partial resonant inverter	
MOSFETS	IRF 540
Diodes	MUR 460
Parallel resonant AC link	
Capacitor	1 µF
Inductor	14 mH
Resonant frequency	1.35 KHz

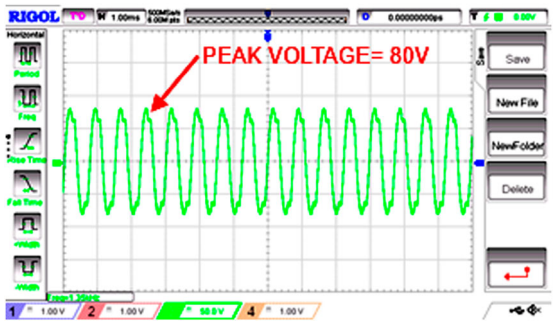

Figure 26. Output Voltage Waveform of Partial Resonant Inverter.

of the nine-level inverter through two diode bridge rectifiers. The single-phase AC load in the prototype is considered to be 60W and the solar PV panel is with a maximum rating of 125W.

The parameters used in the experimental verification are shown in Table 4. Whenever the solar power harvested is more than 60W, the battery is charged and when it is less than 60W, the battery discharges and meets the load requirement. The AC Link voltage is maintained constant. Sliding mode control is incorporated with the PRI to regulate the DC link voltages at the desired levels. The MPPT is achieved by the boost converter controlled by the SMC.

The proposed nine-level inverter uses two cascaded H bridges and these CHBMLIs are individually fed with the DC link capacitors as presented in Figure 24. The voltages of the DC link capacitors are in the ratio of 1:3. By switching the eight power switches using the SHE method a nine-level is obtained at the output of the inverter. The switching angles are calculated by the Hopfield neural network and the obtained switching angles are stored in the lookup table for various modulation indexes. In real-time implementation the pulses are coded inside the microcontroller and then from the

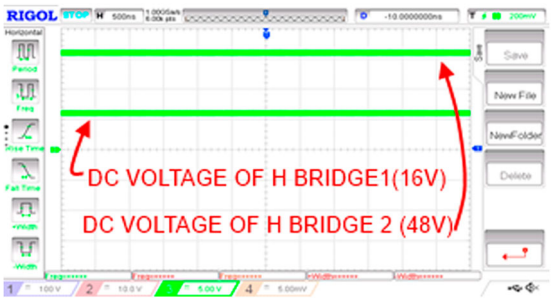

Figure 27. Input DC magnitudes of H bridge 1 and H bridge 2.

microcontroller, the connections are fed to the respective gate driver circuits of the inverter. The maximum voltage level that could be obtained in the cascaded nine-level inverter is $16V + 48V = 64V$. The various voltages obtainable are 0V, 16V, 32V, 48V, and 64V for the positive half cycle and 0V, $-16V$, $-32V$, $-48V$, and $-64V$ for the negative half cycle. For obtaining the nine-level output, four switching instants α_1, α_2, α_3 and α_4 are necessary. These switching instants in the context of step modulation are calculated for every modulation index to be used. The selected switching angles α_1, α_2, α_3 and α_4 guarantee the desired amplitude of the fundamental with the elimination of the lower order harmonics.

Figure 26 presents the output waveform obtained at the Partial Resonant AC link. The root means square (RMS) value of the AC link voltage is obtained as 57 V. By the control implemented in the PRI, the two DC link voltages for the cascaded H bridges have been maintained at 16 and 48 V as shown in Figure 27. Figure 28 presents the experimental output and the THD of the proposed system with the OHSM method. The THD obtained for the proposed system using the OHSM method is 13.73%.

Figure 29 presents the experimental output and the THD of the proposed system with the SHE method. The THD obtained for the proposed system using the SHE method is 5.57%. In Figures 28 and 29(a) the RMS voltage obtained is 45 V. Moreover, from the experimental results, it is observed that the SHE method gives a lesser THD value when compared with the OHSM method.

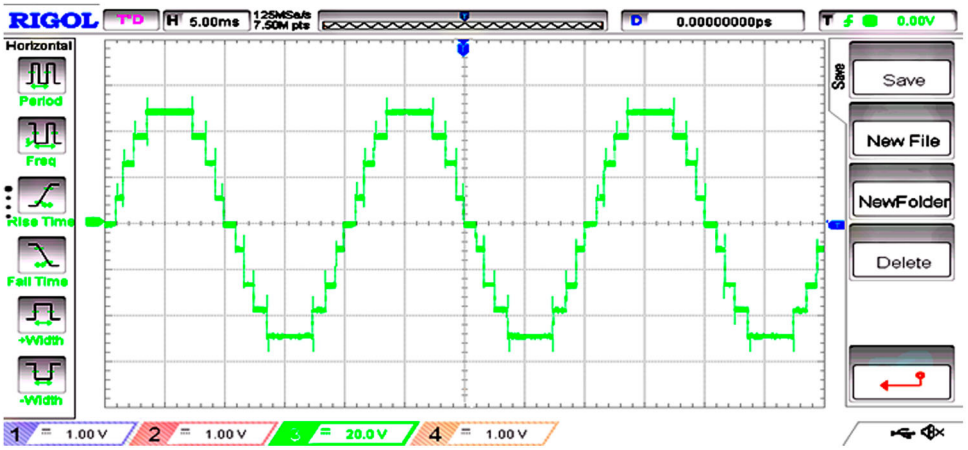

(a)

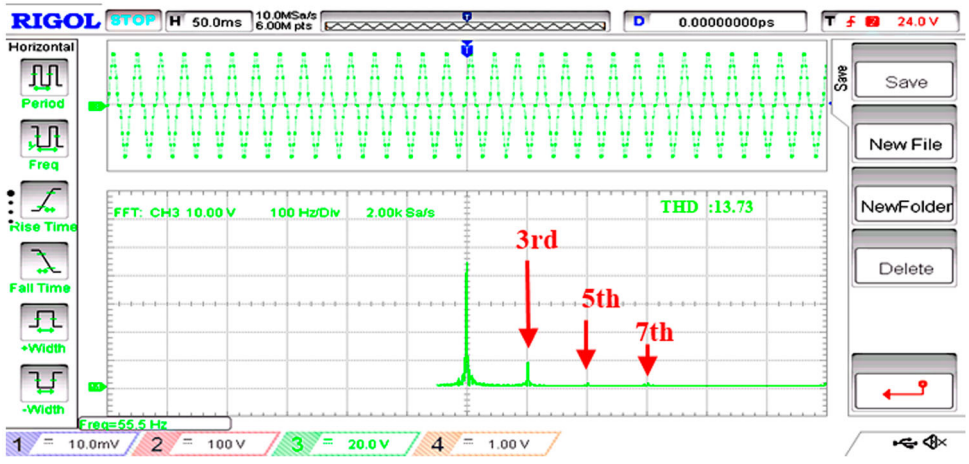

(b)

Figure 28. Experimental output of (a) nine-level inverter with OHSM method (b)THD Spectrum of the Nine Level Inverter with OHSM method.

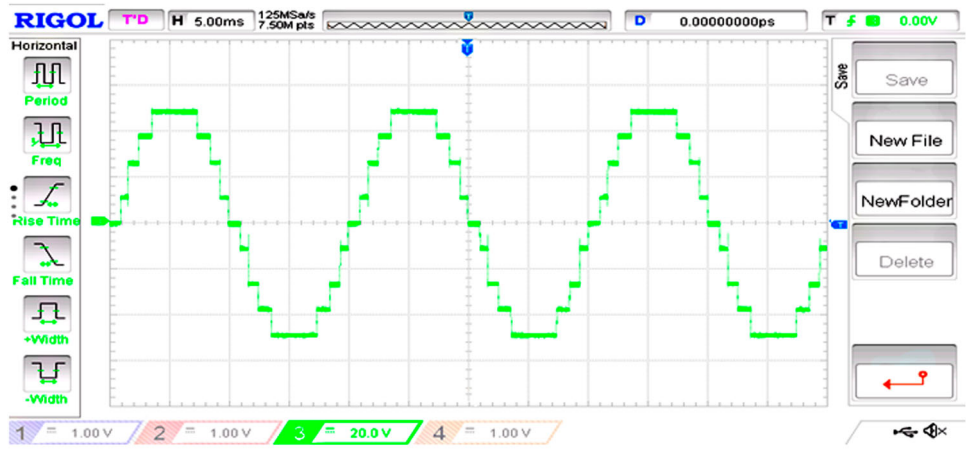

(a)

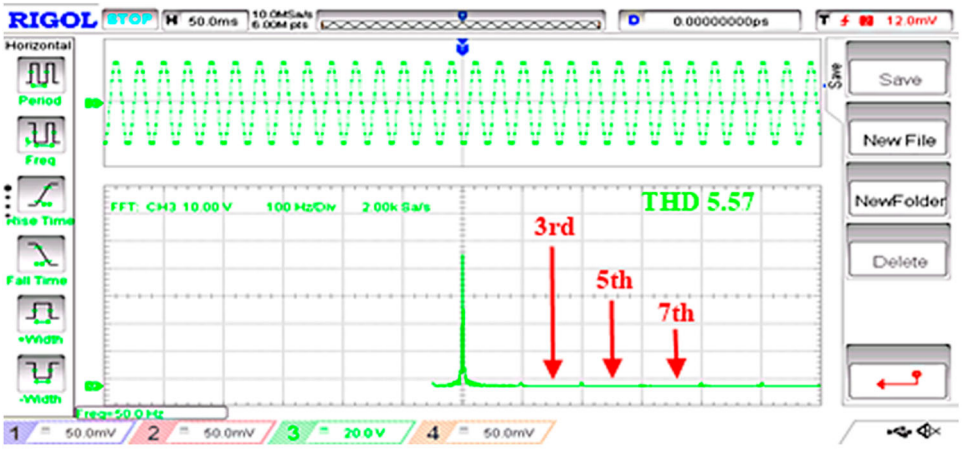

(b)

Figure 29. Experimental output of (a) nine-level inverter with SHE method (b)THD Spectrum of the Nine Level Inverter with SHE method.

10. Conclusion

This paper deals with the PRI based Asymmetrical Cascaded Multilevel Inverter. Implementing the ZVS for the switches of PRI, reduces the requirement of snubber circuit, reduces the switching loss and reduces the switching stress in the proposed system. The DC power is extracted from the PV source using the boost converter and the obtained DC is fed as input to the PRI. The input DC sources of the AMLI is maintained in the ratio of 1:3 to provide a nine-level output. Simulation and Experimental investigations are done for the proposed system using the OHSM and SHE method. The use of SHE for the proposed nine-level inverter has mitigated the selected harmonics of order third, fifth, and seventh. From the results obtained it is concluded that the SHE method gives superior performance when compared to the OHSM method. Finally, the interfacing of PRI with AMLI makes the system compact, reduces the weight of the system, reduces the harmonics in the output and improves the power quality of the system.

Disclosure statement

No potential conflict of interest was reported by the author(s).

Funding

The author(s) reported there is no funding associated with the work featured in this article.

References

[1] Memon MA, Siddique MD, Saad M, et al. Asynchronous particle swarm optimization-genetic algorithm (APSO-GA) based selective harmonic elimination in a cascaded H-bridge multilevel inverter. IEEE Trans Ind Electron. 2021.

[2] Kumawat RK, Palwalia DK. Half bridge module asymmetric multilevel inverter based on novel PWM control strategy. IEEE 6th International Conference on Computer Applications in Electrical Engineering-Recent Advances (CERA); Roorkee, 2017. p. 303–307.

[3] Colak, I., Kabalcı, E., & Keven, G. Asymmetrical multilevel inverter topologies. In Multilevel inverters. Elsevier, London: Academic Press; 2021; p. 181–215.

[4] Ipoum-Ngome PG, Mon-Nzongo DL, Flesch RC, et al. Model predictive current control based on a generalised adjacent voltage vectors approach for multilevel inverters. IET Power Electron. 2019;12(13):3590–3599.
[5] Kumawat RK, Palwalia DK. A comprehensive analysis of reduced switch count multilevel inverter. Aust J Electr Electron Eng. 2019; doi: 10.1080/1448837X.2019.1693884.
[6] Shunmugham Vanaja D, Stonier AA. A novel PV fed asymmetric multilevel inverter with reduced THD for a grid-connected system. Int Trans Electr Energy Syst. 2020;30(4):e12267.
[7] Shunmugham Vanaja D, Albert JR, Stonier AA. An experimental investigation on solar PV fed modular STATCOM in WECS using intelligent controller. Int Trans Electr Energy Syst. 2021;31(5):e12845.
[8] Sinha A, Das MK, Jana KC. Control of asymmetrical cascaded multilevel inverter for a grid-connected photovoltaic system. IET Renew Power Gener. 2019;13(9):1456–1465.
[9] Bana PR, Panda KP, Naayagi RT, et al. Recently developed reduced switch multilevel inverter for renewable energy integration and drives application: topologies, comprehensive analysis and comparative evaluation. IEEE Access. 2019;7:54888–54909.
[10] Shunmugham Vanaja D, Stonier AA. Grid integration of modular multilevel inverter with improved performance parameters. Int Trans Electr Energy Syst. 2021;31(1):e12667.
[11] Bhat AK, Dewan SD. Resonant inverters for photovoltaic array to utility interface. IEEE Trans Aerosp Electron Syst. 1988;24(4):377–386.
[12] Sood PK, Lipo TA. Power conversion distribution system using a resonant high-frequency ac link. 1986. (NASA STI/Recon Technical Report N 86: 25694).
[13] Amirabadi M, Balakrishnan A, Toliyat HA, et al. Soft switched ac-link direct-connect photovoltaic inverter. In 2008 IEEE International Conference on Sustainable Energy Technologies; IEEE; 2008. p. 116–120.
[14] Amirabadi M, Toliyat HA. A new class of PV inverters: series partial resonant converters. In 2012 IEEE Energy Conversion Congress and Exposition (ECCE); IEEE; 2012. p. 3125–3132.
[15] Amirabadi M, Toliyat HA, Alexander WC. A multiport AC link PV inverter with reduced size and weight for stand-alone application. IEEE Trans Ind Appl. 2013;49(5):2217–2228.
[16] Alexander WC. Universal power converter. U.S. Patent 2008/ 0013351A1. 2008 Jan 17.
[17] Amirabadi M, Baek J, Toliyat HA. Sparse ac-link buck–boost inverter. IEEE Trans Power Electron. 2014;29(8):3942–3953.
[18] Amirabadi M, Baek J, Toliyat HA. Ultrasparse AC-link converters. IEEE Trans Ind Appl. 2014;51(1):448–458.
[19] Niapour SA, Mozaffari KH, Amirabadi M. Extremely sparse parallel ac-link universal power converters. IEEE Trans Ind Appl. 2016;52(3):2456–2466.
[20] Kumawat RK, Palwalia DK. Optimization techniques based selective harmonic elimination for multilevel inverter with reduced number of switches. Int J Sci Eng Technol. 2017;6(3):2015–2220.
[21] Satti MB, Hasan A. Direct model predictive control of novel h-bridge multilevel inverter based grid-connected photovoltaic system. IEEE Access. 2019;7:62750–62758.
[22] Kundu S, Burman AD, Giri SK, et al. Comparative study between different optimisation techniques for finding precise switching angle for SHE-PWM of three-phase seven-level cascaded H-bridge inverter. IET Power Electron. 2017;11(3):600–609.
[23] Routray A, Singh RK, Mahanty R. Harmonic minimization in three-phase hybrid cascaded multilevel inverter using modified particle swarm optimization. IEEE Trans Ind Inf. 2018;15(8):4407–4417.
[24] Etesami MH, Farokhnia N, Fathi SH. Colonial competitive algorithm development toward harmonic minimization in multilevel inverters. IEEE Trans Ind Inf. 2015;11(2):459–466.
[25] Priyadarsini R., Selvi B. D. A.. Novel design for reduction of transformer size in Dynamic voltage restorer. Res J Appl Sci Eng Technol; 8(19):2057–2063.
[26] Albert JR, Vanaja DS. Solar energy assessment in various regions of Indian Sub-continent. Solar Cells. IntechOpen, 2020.
[27] Seyedmahmoudian M, Horan B, Soon TK, et al. State of the art artificial intelligence-based MPPT techniques for mitigating partial shading effects on PV systems–a review. Renew Sustain Energy Rev. 2016;64:435–455.
[28] Yap KY, Sarimuthu CR, Lim JMY. Artificial intelligence based MPPT techniques for solar power system: a review. J Mod Power Syst Clean Energy. 2020;8(6):1043–1059. doi:10.35833/MPCE.2020.000159.
[29] Bhat S, Nagaraja HN, Thakur P. DSP based sliding mode control for photovoltaic system. Wirel Pers Commun. 2021;118(4):2219–2237.
[30] Sahoo B, Routray SK, Rout PK. Execution of robust dynamic sliding mode control for smart photovoltaic application. Sustain Energy Technol Assess. 2021;45:101150.
[31] Mohammadhassani F, Narm HG. Dynamic sliding mode control of single-stage boost inverter with parametric uncertainties and delay. IET Power Electron. 2021;18:1–12. https://doi.org/10.1049/pel2.12096.
[32] Balasubramonian M, Rajamani V. Design and real-time implementation of SHEPWM in single-phase inverter using generalized hopfield neural network. IEEE Trans Ind Electron. 2014;61(11):6327–6336.
[33] Sundari MS. Simulation of cascaded H-Bridge multilevel inverter using OHSW PWM for the elimination of harmonics.

Appendix
Switching angle calculation using HNN and solving ODEs with Runge-Kutta 4th order method

```
function [y1,y2,y3,y4] = fcn(m)
%#eml
x = 0;
t=0;
h=0.001;
tp=3.0;
n=(tp-t)/h;
 y1 = 0.7620;
y2 = 1.3043;
y3 = 1.6018;
y4 = 1.6018;
if((m>=0.0)&&(m<.15))
y1 = 0.7620;
y2 = 1.3043;
y3 = 1.6018;
y4 = 1.6018;
 elseif((m>=0.15)&&(m<.25))
y1 =  0.7634;
y2 =  1.2883;
y3 =  1.5955;
y4 = 1.5955;
 elseif((m>=0.25)&&(m<.35))
y1 = 0.7009;
y2 = 1.0689;
y3 = 1.5324;
y4 = 1.5324;
 elseif((m>=0.35)&&(m<.45))
y1 = 0.6668;
y2 = 0.9618;
y3 = 1.3098;
y4 = 1.5868;
 elseif((m>=0.45)&&(m<.55))
y1 = 0.4538;
y2 = 0.9060;
y3 = 1.0953;
y4 = 1.5442;
 elseif((m>=0.55)&&(m<.65))
y1 = 0.4985;
y2 = 0.8482;
y3 = 0.9933;
y4 = 1.2509;
 elseif((m>=0.65)&&(m<.75))
y1 = 0.2497;
y2 = 0.6078;
y3 = 0.8929;
y4 = 1.1778;
 elseif((m>=0.75)&&(m<.85))
y1 = 0.1718;
y2 = 0.3557;
y3 = 0.6703;
y4 = 1.0545;
 elseif((m>=0.85)&&(m<.95))
y1 = 0.0124;
y2 = 0.2476;
y3 = 0.3922;
y4 = 0.6862;
 elseif((m>=0.95)&&(m<=1.0))
y1 = 0.1519;
y2 = 0.1519;
y3 = 0.3998;
y4 = 0.6648;
 end
for i=0:n:1
f1 = function1(y1,y2,y3,y4,m);
k11=h*f1;
 f2 = function2(y1,y2,y3,y4,m);
k12=h*f2;
 f3 = function3(y1,y2,y3,y4,m);
k13=h*f3;
 f4 = function4(y1,y2,y3,y4,m);
k14=h*f4;
   f1 =
function1(y1+k11/2.0,y2+k12/2.0,y3+k13/2
.0,y4+k14/2.0,m);
  k21 = h*f1;
    f2
=function2(y1+k11/2.0,y2+k12/2.0,y3+k13/
2.0,y4+k14/2.0,m);
  k22 = h*f2;
    f3
=function3(y1+k11/2.0,y2+k12/2.0,y3+k13/
2.0,y4+k14/2.0,m);
  k23 = h*f3;
    f4 =
h*function4(y1+k11/2.0,y2+k12/2.0,y3+k13
/2.0,y4+k14/2.0,m);
  k24 = h*f4;
    f1 =
function1(y1+k21/2.0,y2+k22/2.0,y3+k23/2
.0,y4+k24/2.0,m);
  k31 = h*f1;
  f2 =
function2(y1+k21/2.0,y2+k22/2.0,y3+k23/2
.0,y4+k24/2.0,m);
  k32 = h*f2;
  f3
=function3(y1+k21/2.0,y2+k22/2.0,y3+k23/
2.0,y4+k24/2.0,m);
  k33 = h*f3;
  f4 =
function4(y1+k21/2.0,y2+k22/2.0,y3+k23/2
.0,y4+k24/2.0,m);
  k34 = h*f4;
    f1 =
function1(y1+k31,y2+k32,y3+k33,y4+k34,m)
;  k41 = h*f1;
    f2 =
function2(y1+k31,y2+k32,y3+k33,y4+k34,m)
;
  k42 = h*f2;
    f3 =
function3(y1+k31,y2+k32,y3+k33,y4+k34,m)
;
  k43 = h*f3;
    f4 =
function4(y1+k31,y2+k32,y3+k33,y4+k34,m)
;
  k44 = h*f4;
  k1 = (k11+2*(k21+k31)+k41)/6.0;
  k2 = (k12+2*(k22+k32)+k42)/6.0;
  k3 = (k13+2*(k23+k33)+k43)/6.0;
  k4 = (k14+2*(k24+k34)+k44)/6.0;
```

```
%%  prxntf("%5d   %10.6f %10.6f %10.6f
%10.6f %10.6f  %10.6f \n",
x,x,y1,y2,y3,y4,y5);
   x = x  + h;
  y1 = y1 + k1;
  y2 = y2 + k2;
  y3 = y3 + k3;
  y4 = y4 + k4;
  end
 function f1 = function1(y1,y2,y3,y4,m)
f1 = (cos(y1)+cos(y2)+cos(y3)+cos(y4)-
4*m)*sin(y1)...
+(5*cos(5*y1)+5*cos(5*y2)+5*cos(5*y3)+5*
cos(5*y4))*sin(5*y1)...
+(7*cos(7*y1)+7*cos(7*y2)+7*cos(7*y3)+7*
cos(7*y4))*sin(7*y1)...
+(11*cos(11*y1)+11*cos(11*y2)+11*cos(11*
y3)+11*cos(11*y4))*sin(11*y1);
function f2 = function2(y1,y2,y3,y4,m)
f2 = (cos(y1)+cos(y2)+cos(y3)+cos(y4)-
4*m)*sin(y2)...
+(5*cos(5*y1)+5*cos(5*y2)+5*cos(5*y3)+5*
cos(5*y4))*sin(5*y2)...
+(7*cos(7*y1)+7*cos(7*y2)+7*cos(7*y3)+7*
cos(7*y4))*sin(7*y2)...
+(11*cos(11*y1)+11*cos(11*y2)+11*cos(11*
y3)+11*cos(11*y4))*sin(11*y2);
function f3 = function3(y1,y2,y3,y4,m)
f3 = (cos(y1)+cos(y2)+cos(y3)+cos(y4)-
4*m)*sin(y3)...
+(5*cos(5*y1)+5*cos(5*y2)+5*cos(5*y3)+5*
cos(5*y4))*sin(5*y3)...
+(7*cos(7*y1)+7*cos(7*y2)+7*cos(7*y3)+7*
cos(7*y4))*sin(7*y3)...
+(11*cos(11*y1)+11*cos(11*y2)+11*cos(11*
y3)+11*cos(11*y4))*sin(11*y3)
function f4 = function4(y1,y2,y3,y4,m)
f4 = (cos(y1)+cos(y2)+cos(y3)+cos(y4)-
4*m)*sin(y3)...
+(5*cos(5*y1)+5*cos(5*y2)+5*cos(5*y3)+5*
cos(5*y4))*sin(5*y3)...
+(7*cos(7*y1)+7*cos(7*y2)+7*cos(7*y3)+7*
cos(7*y4))*sin(7*y3)...
+(11*cos(11*y1)+11*cos(11*y2)+11*cos(11*
y3)+11*cos(11*y4))*sin(11*y3);
```